Mathematics

FINITE ELEMENT ANALYSIS AS COMPUTATION

What the textbooks don't teach you about finite element analysis

Chapter 7:

Membrane locking, parasitic shear and incompressible locking

Gangan Prathap
Director
NISCAIR, S.V. Marg
New Delhi - 110016

Contents

Chapter 7

Membrane locking, parasitic shear and incompressible locking

7.1 Introduction

The *shear locking* phenomenon was the first of the *over-stiffening behavior* that was classified as a locking problem. Other such pathologies were noticed in the behavior of curved beams and shells, in plane stress modeling and in modeling of three dimensional elastic behavior at the incompressible limit *($\nu \to 0.5$)*. The field-consistency paradigm now allows all these phenomena to be traced to inconsistent representations of the constrained strain fields. A unifying pattern is therefore introduced to the understanding of the locking problems in constrained media elasticity - whether it is shear locking in a straight beam or flat plate element, membrane locking in a curved beam or shell element, parasitic shear in 2D plane stress and 3D elasticity or incompressible locking in 2D plane strain and 3D elasticity as the Poisson's ratio $\nu \to 0.5$.

This chapter will now briefly summarize this interpretation. Unlike the chapter on shear locking, a detailed analysis is omitted as it would be beyond the scope of the present book and readers should refer to the primary published literature.

7.2 Membrane locking

Earlier, we argued that the most part of structural analysis deals with the behavior of thin flexible structures. One popular and efficient form of construction of such thin flexible structures is the shell - enclosing space using one or more curved surfaces. A shell is therefore the curved form of a plate and its structural action is a combination of stretching and bending. It is possible to perform a finite element analysis of a shell by using what is called a facet representation - i.e. the shell surface is replaced with flat triangular and/or quadrilateral plate elements in which a membrane stiffness (membrane element) is superposed on a bending stiffness (plate bending element). Such a model is understandably inaccurate in that with very coarse meshes, they do not capture the bending-stretching coupling of thin shell behavior. Hence, the motivation for designing elements with mid-surface curvature taken into account and which can capture the membrane-bending coupling correctly. There are two ways in which this could be done. One is to use elements based on specific shell theories (e.g. the Donnell, Flugge, Sanders, Vlasov theories, etc.). There are considerable controversies regarding the relative merits of these theories as each has been obtained by carrying out approximations to different degrees when the 3-dimensional field equations are reduced to the particular class of shell equations. The second approach is called the degenerate shell approach - three dimensional solid elements can be reduced (degenerated) into shell elements having only mid-surface nodal variables - these are no longer dependent on the various forms of shell theories proposed and should be simple to use. They are in fact equivalent to a Mindlin type curved shell element.

However, accurate and robust curved shell elements have been extremely difficult to design - a problem challenging researchers for nearly three decades. One key issue behind this difficulty is the phenomenon of membrane locking - the very poor behavior of curved elements, as they become thin. This

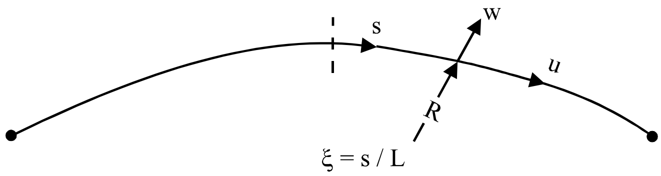

Fig. 7.1 The classical thin curved beam element.

was neither recognized nor understood for a very long time. It was believed at first that this was because curved elements could not satisfy the *strain-free rigid body motion condition* because of their inherent curved geometry. In this section, we shall apply the field-consistency paradigm to the problem to recognize that a consistent representation of membrane strains is desired to avoid the phenomenon called membrane locking and that it is the need for *consistency* rather than the requirement for *strain-free rigid body motion* which is the key factor. This is most easily identified by working with the one-dimensional curved beam (or arch) elements.

In Chapter 6, we studied structural problems where both bending and shear deformation was present. We saw that simple finite element models for the shear deformable bending action of a beam or plate behaved very poorly in thin beam or plate regimes where the shear strains become vanishingly small when compared with the bending strains. This phenomenon is known as *shear locking*. We also saw how the field-consistency paradigm was needed to explain this behavior in a scientifically satisfying way.

We shall now see that a similar problem appears in curved finite elements in which both flexural and membrane deformation take place. Such elements perform very poorly in cases where inextensional bending of the curved structure was predominant, i.e. the membrane strains become vanishingly small when compared to the bending strains. This phenomenon has now come to be called *membrane locking*.

In this section, we shall examine in turn, the classical thin curved beam element and the linear and quadratic shear flexible curved beam elements in a curvilinear co-ordinate system.

7.2.1 The classical thin curved beam element

Figure 7.1 describes the simplest curved beam element of length *2l* and radius of curvature *R* based on classical thin beam theory. The displacement degrees of freedom required are the circumferential displacement *u* and the radial displacement *w*. The co-ordinate *s* follows the middle line of the curved beam. The membrane strain ε and the bending strain χ are described by the strain-displacement relations

$$\varepsilon = u,_s + w/R \qquad (7.1a)$$

$$\chi = u,_s/R - w,_{ss} \qquad (7.1b)$$

A C^0 description for *u* and a C^1 description *w* is required. Kinematically admissible displacement interpolations for *u* and *w* are

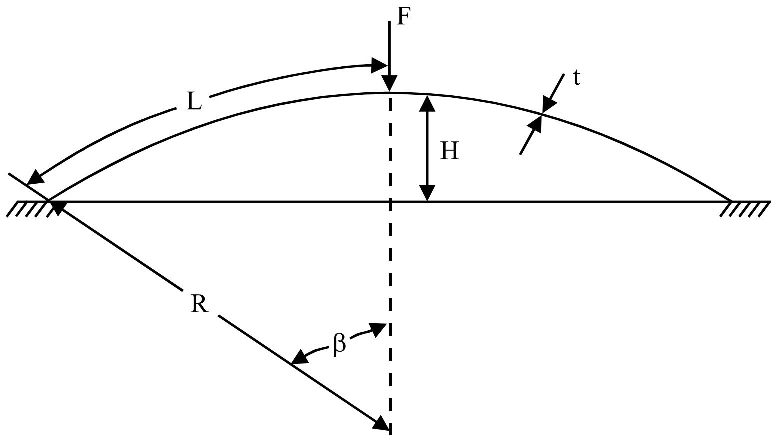

Fig. 7.2 Geometry of a circular arch

$$u = a_0 + a_1\xi \tag{7.2a}$$

$$w = b_0 + b_1\xi + b_2\xi^2 + b_3\xi^3 \tag{7.2b}$$

where $\xi = s/l$ and a_0 to b_3 are the generalized degrees of freedom which can be related to the nodal degrees of freedom u, w and $w_{,s}$ at the two nodes.

The strain field interpolations can be derived as

$$\chi = \left(a_1/Rl - 2b_2/l^2\right) - \left(6b_3/l^2\right)\xi \tag{7.3a}$$

$$\varepsilon = \left(a_1/l + b_0/R + b_2/3R\right) + \left(b_1/R + 3b_3/5R\right)\xi - b_2/3R\left(1 - 3\xi^2\right) - b_3/5R\left(3\xi - 5\xi^3\right) \tag{7.3b}$$

If a thin and deep arch (i.e. having a large span to rise ratio so that $L/t>>1$ and R/H is small, see Fig. 7.2) is modeled by the curved beam element, the physical response is one known as inextensional bending such that the membrane strain tends to vanish. From Equation (7.3b) we see that the inextensibility condition leads to the following constraints:

$$a_1/l + b_0/R + b_2/3R \to 0 \tag{7.4a}$$

$$b_1 + 3b_3/5 \to 0 \tag{7.4b}$$

$$b_2 \to 0 \tag{7.4c}$$

$$b_3 \to 0 \tag{7.4d}$$

Following the classification system we introduced earlier, we can observe that constraint (7.4a) has terms participating from both the u and w fields. It can therefore represent the condition $\varepsilon = u_{,s} + w/R \to 0$ in a physically meaningful way, i.e. it is a *true constraint*. However, the three remaining constraint (7.4b) to (7.4d) have no participation from the u field. Let us now examine in turn what these three constraints imply for the physical problem. From the three constraints we have the conditions $b_1 \to 0$, $b_2 \to 0$ and $b_3 \to 0$. Each in turn implies the conditions $w_{,s} \to 0$, $w_{,ss} \to 0$ and $w_{,sss} \to 0$. These are the *spurious constraints*.

This element has been studied extensively and the numerical evidence given there confirms that membrane locking is mainly determined by the first of these three constraints. Next, we shall briefly describe the functional re-constitution analysis that will yield semi-quantitative error estimates for membrane locking in this element.

We can now use the functional re-constitution technique, (which in Chapter 6 revealed how the discretization process associated with the linear Timoshenko beam element led to large errors known as shear locking) to see how the inconsistent constraints in the membrane strain field interpolation (Equations (7.4b) to (7.4d)) modify the physics of the curved beam problem in the discretization process.

The analysis is a little more difficult than for the shear locking case and would not be described in full here. For a curved beam of length *2l*, moment of inertia *I* and area of cross-section *A*, the strain energy can be written as,

$$\pi_e = \int \left(1/2\, EI\, \chi^T \chi + 1/2\, EA\, \varepsilon^T \varepsilon \right) ds \tag{7.5}$$

where ε and χ are as defined in Equation (7.1). For simplicity assume that the cross-section of the beam is rectangular so that if the depth of the beam is *t*, then $I = At^2/12$. After discretisation, and reconstitution of the functional, we can show that the inconsistent membrane energy terms disturb the bending energy terms - the principal stiffening term is physically equivalent to a spurious in-plane or membrane stiffening action due to an axial load $N = \left(EA\, l^2/3R^2 \right)$.

This action is quite complex and it is not as simple to derive useful universally valid error estimates as was possible with the linear Timoshenko beam element. We therefore choose a problem of simple configuration which can reveal the manner in which the membrane locking action takes place. We consider a shallow circular arch of length *L* and radius of curvature *R*, simply supported at the ends. The loading system acting on it is assumed to induce nearly inextensional bending. We also assume that the transverse deflection *w* can be approximated in the form $w=c\sin(\pi s/L)$. If the entire arch is discretized by curved beam elements of length *2l* each, the strain energy of the discretized arch (again assuming that $\chi=-w_{,ss}$ and neglecting the consistently modeled part of the membrane energy) one can show that due to membrane locking, the bending rigidity of the arch has now been altered in the following form:

$$(EI)' / (EI) = \left\{ 1 + \left(4/\pi^2 \right) \left(L\, l/Rt \right)^2 \right\} \tag{7.6}$$

We can therefore expect membrane locking to depend on the structural parameter of the type $(Ll/Rt)^2$.

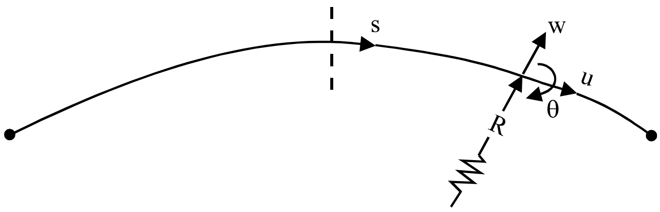

Fig. 7.3 The Mindlin curved beam element.

Numerical experiments with various order integration rules applied to evaluate the various components of the stiffness matrix indicated that the inconsistent elements locked exactly as predicted by the pattern describe above. The consistent element was entirely free of locking.

This classical curved beam element (the cubic-linear element) was discredited for a very long time because it was not possible to understand why the element should perform so poorly. We have now found that the explanation for its very poor behavior could be attributed entirely to the inconsistency in the membrane strain field interpolations. The belief that the lack of the strain free rigid body motion in the conventional formulation was the cause of these errors cannot be substantiated at all. We have also seen how we could restore the element into a very accurate one (having the accuracy of the straight beam models) by designing a new membrane strain field which met the *consistency* requirements.

7.2.2 The Mindlin curved beam elements

The exercise above showed that the locking behavior of curved beams could be traced to the inconsistent definition of the membrane strain field. The curved beam element used to demonstrate this was based on classical thin beam theory and used a curvilinear co-ordinate description. Of interest to us now is to understand how the membrane locking phenomenon can take place in a general curved shell element. Most general shell elements which have now been accepted into the libraries of general purpose finite element packages are based on what is called the degenerate shell theory which is equivalent to a shear deformable theory and use quadratic interpolations (i.e. three nodes on each edge to capture the curved geometry in a Cartesian system).

To place the context of membrane locking in general shell elements correctly, it will be useful to investigate the behavior of the Mindlin curved beam elements. These are now described by the circumferential (tangential) displacement u, the radial (normal) displacement w and the rotation of a normal to the midline θ. As in the Timoshenko beam element, this rotation differs from the rotation of the mid-line $w,_s$ by an amount $\gamma = \theta - w,_s$ which describes the shear strain at the section. Fig. 7.3 shows how the Mindlin curved beam element is specified.

The strain energy in a Mindlin curved beam is $U=U_M+U_B+U_S$ where the respective contributions to U arise from the membrane strain ε, the bending strain χ and the transverse shear strain γ. For an element of length $2l$ and radius R,

$$U_M = (1/2)(EA)\int \varepsilon^2 \, ds \quad \text{where } \varepsilon = u,_s + w/R \qquad (7.7a)$$

$$U_B = (1/2)(EI)\int \chi^2 \, ds \text{ where } \chi = u_{,s}/R - \theta_{,s} \tag{7.7b}$$

$$U_S = (1/2)(kGA)\int \gamma^2 \, ds \text{ where } \gamma = \theta - w_{,s} \tag{7.7c}$$

where *EA, EI* and *kGA* represent the respective rigidities.

There are no difficulties with the bending strain. However, depending on the regime, both shear strains and membrane strains can be constrained to vanish leading to shear and membrane locking. The arguments concerning shear locking are identical to those expressed in Chapter 6, i.e. while the inconsistency in the shear strain field is severe enough to cause locking in the former (a significant stiffening which caused errors that propagated indefinitely as the structural parameter kGl^2/Et^2 became very large), it is much milder in the latter and is responsible only for a poorer rate of convergence (the performance of the element having reduced to that of the linear field-consistent element). However with membrane locking, the inconsistencies at the quadratic level can cause locking - therefore both the linear and quadratic elements must be examined in turn to get the complete picture.

For the linear Mindlin curved beam element, as a C^0 displacement type formulation is sufficient, we can choose linear interpolations of the following form,

$$u = a_0 + a_1\xi \tag{7.8a}$$

$$w = b_0 + b_1\xi \tag{7.8b}$$

$$\theta = c_0 + c_1\xi \tag{7.8c}$$

where $\xi = s/l$ is the natural co-ordinate along the arch mid-line. These interpolations lead to the following membrane strain field interpolation:

$$\varepsilon = (a_1/l + b_0/R) + (b_1/R)\,\xi \tag{7.9}$$

There is now one single spurious constraint in the limit of inextensional bending of an arch, i.e. $b_1 \to 0$, which implies a constraint of the form $w_{,s} \to 0$ at the centroid of the element. The membrane locking action is similar to but simpler than that seen for the classical thin curved beam element above. In a thin beam, in the Kirchhoff limit, $\theta \to w_{,s}$, which implies that membrane locking induces the section rotations θ to lock. It can therefore be seen that a constraint of this form leads to an in-plane stiffening action of the form corresponding to the introduction of a spurious energy

$$(1/2)\left(EAl^2/3R^2\right)\int w_{,s}{}^2 ds \tag{7.10}$$

The membrane locking action is therefore identical to that predicted for the classical thin curved beam. A variationally correct field-consistent element can easily be derived using the Hu-Washizu theorem. This is a very accurate element.

The quadratic Mindlin curved beam element can also be interpreted in the light of our studies of the classical curved beam earlier. Spurious constraints at both the linear (i.e. $w_{,s} \to 0$) and quadratic (i.e $w_{,ss} \to 0$) levels lead to errors that propagate at a $(L\,l/Rt)^2$ rate and $\left(l^2/Rt\right)^2$ rate respectively. We expect now that in a quadratic Mindlin curved beam element, the latter constraint is the one that is present and that these errors are large enough to make the membrane locking effect noticeable. This also explains why the degenerate shell elements, which are based on quadratic interpolations, suffer from membrane locking.

A quadratic (three-node) element having nodes at $s=-l$, 0 and l (see Fig. 7.3) would have a displacement field specified as,

$$u = a_0 + a_1\xi + a_2\xi^2 \tag{7.11a}$$
$$w = b_0 + b_1\xi + b_2\xi^2 \tag{7.11b}$$
$$\theta = c_0 + c_1\xi + c_2\xi^2 \tag{7.11c}$$

The membrane strain field can be expressed as:

$$\varepsilon = (a_1/l + b_0/R + b_2/3R) + (2a_2/l + b_1/R)\,\xi - b_2/3R\left(1-3\xi^2\right) \tag{7.12}$$

The spurious constraint is now $b_2 \to 0$ a discretized equivalent of imposing the constraint $w,_{ss} \to 0$ at the centroid of each element. To understand that this can cause locking, we note that in a thin curved beam, $\theta,_s \to w,_{ss}$ and therefore a spurious constraint of this form acts to induce a spurious bending energy. A functional re-constitution approach will show that the bending energy for a thin curved beam modifies to,

$$U_B = (1/2)(EI)\int\left[1 + (4/15)\left(l^2/Rt\right)^2\right] w,_{ss}^2\, ds \tag{7.13}$$

This can be interpreted as spurious additional stiffening of the actual bending rigidity of the structure by the $(4/15)\left(l^2/Rt^2\right)$ term. It is a factor of this form that caused the very poor performance of the exactly integrated quadratic shell elements.

A variationally correct field consistent element is obtained by using the Hu-Washizu theorem or very simply by using a two-point integration rule for the shear and membrane strain energy energies. This is an extremely accurate element. It is interesting to compare the error norm for locking for this element, i.e. $\left(l^2/Rt^2\right)$ with the corresponding error norm for locking in the inconsistent linear Mindlin curved beam element, which is $\left(L\,l/Rt^2\right)$. It is clear that since $L>>l$ when an arch is discretized with several elements, the locking in the quadratic element is much less than in the linear element. One way to look at this is to examine the rate at which locking is relieved as more elements are added to the mesh, i.e. as l is reduced. In the case of the inconsistent linear element, locking is relieved only at an l^2 rate whereas in the case of the quadratic element, locking is relieved at the much faster l^4 rate. However, locking in the quadratic element is significant enough to degrade the performance of the quadratic curved beam and shell elements to a level where it is impractical to use in its inconsistent form. This is clearly seen from the fact that to reduce membrane-locking effects to acceptable limits, one must use element lengths $l << \sqrt{Rt}$. Thus for an arch with $R=100$ and $t=1$, one must use about a *100* elements to achieve an accuracy that can be obtained with two to four field-consistent elements.

7.2.3 Axial force oscillations

Our experience with the linear and quadratic straight beam elements showed that inconsistency in the constrained strain-field is accompanied by spurious stress oscillations corresponding to the inconsistent constraints. We can now understand that the inconsistent constraint $b_1 \to 0$ will induce linear axial force oscillations in the linear curved beam element. Similarly, the inconsistent quadratic constraint will trigger off quadratic oscillations in the quadratic element.

7.2.4 Concluding remarks

So far, we have examined the phenomenon of membrane locking in what were called the *simple* curved beam elements. These were based on curvilinear geometry and the membrane locking effect was easy to identify and quantify. However, curved beam and shell elements which are routinely used in general purpose finite element packages are based on quadratic formulations in a Cartesian system. We shall call these the *general* curved beam and shell elements. Membrane locking is not so easy to anticipate in such a formulation although the predictions made in this section have been found to be valid for such elements.

7.3 Parasitic shear

Shear locking and membrane locking are phenomena seen in finite element modeling using structural elements based on specific theories, e.g. beam, plate and shell theories. These are theories obtained by simplifying a more general continuum description, e.g. the three dimensional theory of elasticity or the two dimensional theories of plane stress, plane strain or axisymmetric elasticity. The simplifications are made by introducing restrictive assumptions on strain and/or stress conditions like vanishing of shear strains or vanishing of transverse normal strains, etc. In the beam, plate and shell theories, this allows structural behavior to be described by mid-surface quantities. However, these restrictive assumptions impose constraints which make finite element modeling quite difficult unless the consistency aspects are taken care of. We shall now examine the behavior of *continuum* elements designed for modeling continuum elasticity directly, i.e. 2D elements for plane strain or stress or axisymmetric elasticity and solid elements for 3D elasticity. It appears that

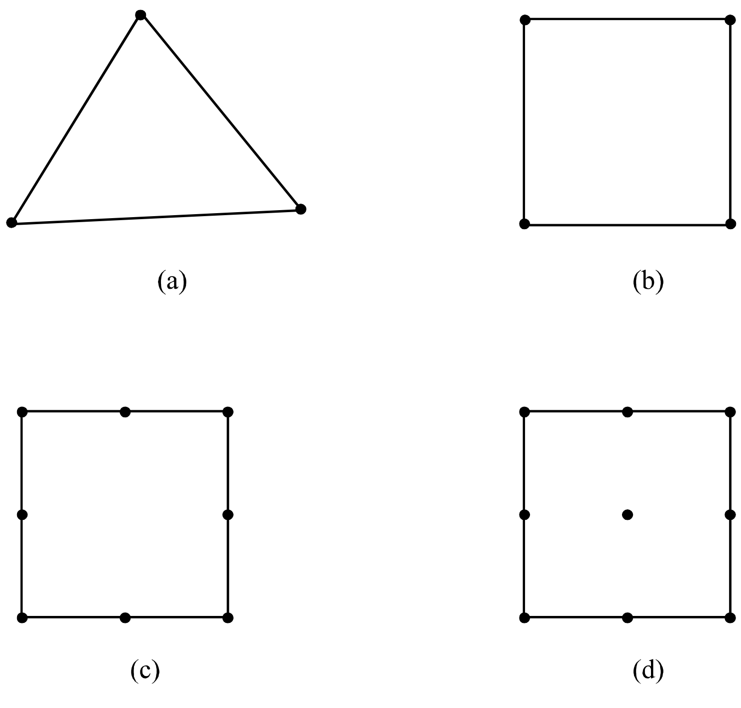

Fig. 7.4 (a) Constant strain triangle, (b) Rectangular bilinear element, (c) Eight-node rectangle and (d) Nine-node rectangle.

under constraining physical regimes, locking behavior is possible. One such problem is *parasitic shear*. We shall see the genesis of this phenomenon and show that it can be explained using the consistency concepts. The problems of *shear locking*, *membrane locking* and *parasitic shear* obviously are very similar in nature and the unifying factor is the concept of consistency.

The finite element modeling of plane stress, plane strain, axisymmetric and 3D elasticity problems can be made with two-dimensional elements and three-dimensional elements (sometimes called continuum elements to distinguish them from structural elements), of which the linear 3-noded triangle and bi-linear 4- noded rectangle (Fig. 7.4) are the simplest known in the 2D case. In most applications, these elements are reliable and accurate for determining general two-dimensional stress distributions and improvements can be obtained by using the higher order elements, the quadratic 6-noded triangle and 8- or 9-noded quadrilateral elements (Fig. 7.4).

However, in some applications, e.g. the plane stress modeling of beam flexure or in plane strain and axisymmetric applications where the Poisson's ratio approaches 0.5 (for nearly incompressible materials or for materials undergoing plastic deformation), considerable difficulties are seen. *Parasitic shear* occurs in the plane stress and 3D finite element modeling of beam flexure. Under pure bending loads, for which the shear stress should be zero, the elements yield large values of shear stress except at certain points (e.g. centroids in linear elements). In the linear elements, the errors progress in the same fashion as for shear locking in the linear Timoshenko beam element, i.e. the errors progress indefinitely as the element aspect ratio increases. Reduced integration of the shear strain energy or addition of bubble modes for the 4-noded

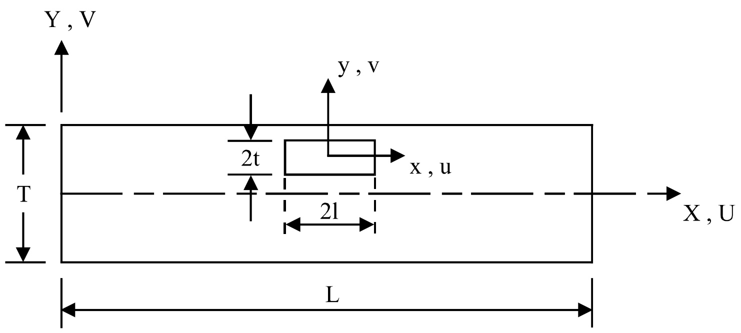

Fig. 7.5 Plane stress model of beam flexure.

rectangular element completely eliminates this problem. The 8- and 9-noded elements do not lock but improve in performance with reduced integration. These elements, in their original (i.e. field-inconsistent) form show severe linear and quadratic shear stress oscillations.

Here, we shall extend the consistency paradigm to examine this phenomenon in detail, confining attention to the rectangular elements.

7.3.1 Plane stress model of beam flexure

Figure 7.5 shows a two-dimensional plane stress description of the problem of beam flexure. The beam is of length L, depth T and thickness (in the normal to the plane direction) b. Two independent field variables are required to describe the problem, the displacements u and v (Fig. 7.5). The strain energy functional for this problem consists of energies from the normal strains, U_E and shear strains, U_G. For an isotropic case, where *E* is the Young's modulus, *G* is the shear modulus and ν is Poisson's ratio,

$$U = U_E + U_G$$

$$= \int_0^L \int_0^T \left[\frac{Eb}{2\left(1-\nu^2\right)} \left(u^2{}_{,x} + v^2{}_{,y} + 2\nu\, u_{,x}\, v_{,y} \right) + Gb/2 \left(u_{,y} + v_{,x} \right)^2 \right] dx\, dy \qquad (7.14)$$

A one-dimensional beam theory can be obtained by simplifying this problem. For a very slender beam, the shear strains must vanish and this would then yield the classical Euler-Bernouilli beam theory. Note that although shear strains vanish, shear stresses and shear forces would remain finite. We shall see now that it is this constraint condition that leads to difficulties in plane stress finite element modeling of such problems.

7.3.2 The 4-node rectangular element

An element of length *2l* and depth *2t* is chosen. The rectangular form is chosen so that the issues involved can be identified clearly. There are now 8 degrees of freedom, u_1-u_4 and v_1-v_4 at the four nodes. The field-variables are now interpolated in the following fashion:

$$u = a_0 + a_1 x + a_2 y + a_3 xy \qquad (7.15a)$$
$$v = b_0 + b_1 x + b_2 y + b_3 xy \qquad (7.15b)$$

We need to examine only the shear strain field that will become constrained (i.e. become vanishingly small) while modeling the flexural action of a thin beam. This will be interpolated as,

$$\gamma = u_{,y} + v_{,x} = \left(a_2 + b_1\right) + a_3 x + b_3 y \qquad (7.16)$$

and the shear strain energy within the element will be,

$$U_e(G) = \int_{-l}^{l} \int_{-t}^{t} Gb/2 \left(a_2 + b_1 + a_3 x + b_3 y\right)^2 dx\, dy$$
$$= (Gb/2)(4t\,l) \left[\left(a_2 + b_1\right)^2 + \left(a_3 l\right)^2/3 + \left(b_3 t\right)^2/3 \right] \qquad (7.17)$$

Equation (7.17) suggests that in the thin beam limit, the following constraints will emerge:

$$a_2 + b_1 \to 0 \qquad (7.18a)$$
$$a_3 \to 0 \qquad (7.18b)$$
$$b_3 \to 0 \qquad (7.18c)$$

We can see that Equation (7.18a) is a constraint that comprises constants from both *u* and *v* functions. This can enforce the true constraint of vanishing shear strains in a realistic manner. In contrast, Equations (7.18b) and (7.18c) impose constraints on terms from one field function alone in each case. These are undesirable constraints. We shall now see how these lead to the stiffening effect that is called parasitic shear.

In the plane stress modeling of a slender beam, we would be using elements which are very long in the x direction, i.e. elements with $l>t$ would be used. One can then expect from Equation (7.17) that as $l^2>>t^2$, the constraint $a_3\to 0$ will be enforced more rapidly than the constraint $b_3\to 0$ as the beam becomes thinner. The spurious energies generated from these two terms will also be in a similar proportion. In Equation (7.17), one can interpret the shear strain field to comprise a constant value, which is *`field-consistent'* and two linear variations which are *`field-inconsistent'*. We see now that the variation along the beam length is the critical term. Therefore, let us consider the use of the shear strain along $y=0$ as a measure of the averaged shear strain across a vertical section. This gives

$$\gamma = (a_2 + b_1) + a_3 x \tag{7.19}$$

Thus, along the length of the beam element, γ have a constant term that reflects the averaged shear strain at the centroid, and a linear oscillating term along the length, which is related to the spurious constraint in Equation (7.18b). As in the linear beam element in Section 4.1.6, this oscillation is self-equilibrating and does not contribute to the force equilibrium over the element. However, it contributes a finite energy in Equation (7.17) and in the modeling of very slender beams, this spurious energy is so large as to completely dominate the model of the beam behavior and cause a locking effect. We shall now use the functional re-constitution technique to determine the magnitude of locking and the extent of the shear stress oscillations triggered off by the inconsistency in the shear strain field.

We shall simplify the present example and derive the error estimates from the functional re-constitution exercise. We shall denote by $\bar{a}_3$, the coefficient determined in a solution of the beam problem by using a field-consistent representation of the total energy in the beam, and by a_3, the value from a solution using energies based on inconsistent terms. The field-consistent and field-inconsistent terms will differ by,

$$\bar{a}_3 / a_3 = \left(1 + Gl^2 / Et^2\right) \tag{7.20}$$

This factor, $e_L = \left(1 + Gl^2 / Et^2\right)$ is the additional stiffening parameter that determines the extent of parasitic shear.

We can relate a_3 to the physical parameters relevant to the problem of a beam in flexure to show that if $e_L >> 1$, as in a very slender beam, there are shear force oscillations,

$$V = V_0 + \left(3M_0 / l\right)\left(x / l\right) \tag{7.21}$$

The oscillations are proportional to the centroidal moment, and for $e_L >> 1$, the oscillations are inversely proportional to the element length, i.e. they become more severe for smaller lengths of the plane stress element. It is important to note that a field-inconsistent two node beam element based on linear interpolations for w and θ (see Equation (7.19)) produces an identical stress oscillation.

7.3.3 The field-consistent elements

It is well known that the plane stress elements behave reliably in general 2D applications where no constraints are imposed on the normal or shear strain fields. The need for field-consistency becomes important only when a strain field is constrained. Earlier, we saw that in the plane stress modeling of thin beam flexure, the shear strain field is constrained and that these constraints are enforced by a penalty multiplier Gl^2/Et^2 . The larger this term is, the more severely constrained the shear strain becomes. Of the many strategies that are available for removing the spurious constraints on the shear strain field, the use of a variationally correct re-distribution is recommended. This requires the field-consistent $\bar{\gamma}$ to be determined from γ using the orthogonality condition

$$\int \delta\bar{\gamma}^T \left(\bar{\gamma} - \gamma\right) dx\ dy = 0 \tag{7.22}$$

Thus instead of Equation (7.16), we can show that the shear strain-field for the 4-node rectangular plane stress element will be,

$$\bar{\gamma} = \left(a_2 + b_1\right) \tag{7.23}$$

It is seen that the same result is achieved if reduced integration using a *1* Point Gaussian integration is applied to shear strain energy evaluation. In a very similar fashion, the consistent shear strain field can be derived for the quadratic elements.

7.3.4 Concluding remarks on the rectangular plane stress elements

The field-consistency principle and the functional re-constitution technique can be applied to make accurate error analyses of conventional 4-node and 8-node plane stress elements. These *a priori* estimates have been confirmed through numerical experiments.

A field-consistent re-distribution strategy allows these elements to be free of locking and spurious stress-oscillations in modeling flexure. These options can be built into a shape function sub-routine package in a simple manner so that where field-consistency requirements are paramount, the appropriate smoothed shape functions will be used.

7.3.5 Solid element model of beam/plate bending

So far, we have dealt with the finite element modeling of problems which were simplified to one-dimensional or two-dimensional descriptions. There remains a large class of problems which need to be addressed directly as three dimensional states of stress. Solid or three dimensional elements are needed to carry out the finite element modeling of such cases. A variety of 3D solid elements exist, e.g. tetrahedral, triangular prism or hexahedral elements. In general cases of 3D stress analysis, no problems are encountered with the use of any of these elements as long as a sufficiently large number of elements are used and no constrained media limits are approached. However, under such limits the tetrahedral and triangular prism elements cannot be easily modified to avoid these difficulties. It is possible however to improve the hexahedral 8-node and 27-node elements so that they are free of locking and of other ill-effects like stress oscillations. One problem encountered is that of *parasitic shear* or *shear locking* when solid elements are used to model regions where bending action is predominant. In fact, in such models, *parasitic shear* and *shear locking* merge indistinguishably into each other. We briefly examine this below.

The 8-noded brick element is based on the standard tri-linear interpolation functions and is the three dimensional equivalent of the bi-linear plane stress element. It would appear now that the stiffness matrix for the element can be derived very simply by carrying out the usual finite element operations, i.e. with strain-displacement matrix, stress-strain matrix and numerically exact integration (i.e. $2\times2\times2$ Gaussian integration). Although this element performs very well in general 3D stress analysis, it failed to represent cases of pure bending (parasitic shear) and cases of near incompressibility (incompressible locking).

The element is unable to represent the shear strains in a physically meaningful form when the shear strains are to be constrained, as in a case of pure bending. The phenomenon is the 3D analogue of the problem we noticed for the bi-linear plane stress element above. The problem of designing a useful 8-node brick element has therefore received much attention and typical attempts to alleviate this have included techniques such as reduced integration, addition of bubble functions and assumed strain hybrid formulations. We shall now look at this from the point of view of consistency of shear strain interpolation.

We can observe here that the shear strain energy is computed from Cartesian shear strains γ_{xy}, γ_{xz} and γ_{yz}. In the isoparametric formulation, these are to be computed from terms involving the derivatives of *u, v, w* with respect to the natural co-ordinates ξ, η, ζ and the terms from the inverse of the three dimensional Jacobian matrix. It is obvious that it will be a very difficult, if not impossible task, to assure the consistency of the interpolations for the Cartesian shear strains in a distorted hexahedral. Therefore attention is confined to a regular hexahedron so that consistency requirements can be easily examined.

To facilitate understanding, we shall restrict our analysis to a rectangular prismatic element so that the (x, y, z) and (ξ, η, ζ) systems can be used interchangeably. We can consider the tri-linear interpolations to be expanded in the following form, i.e.

$$u = a_1 + a_2x + a_3y + a_4z + a_5xy + a_6yz + a_7xz + a_8xyz \tag{7.24a}$$
$$v = b_1 + b_2x + b_3y + b_4z + b_5xy + b_6yz + b_7xz + b_8xyz \tag{7.24b}$$
$$w = c_1 + c_2x + c_3y + c_4z + c_5xy + c_6yz + c_7xz + c_8xyz \tag{7.24c}$$

where a_1 to a_8 and b_1 to b_8 are related to the nodal degrees of freedom u_1 to u_8 and v_1 to v_8 respectively. We shall now consider a case of a brick element undergoing a pure bending response requiring a constrained strain field $\gamma_{xy} = u,_y + v,_x \to 0$. From Equations (7.24a) and (7.24b) we have,

$$\gamma_{xy} = (a_3 + b_2) + (a_6 + b_7)z + a_5x + b_5y + a_8xz + b_8yz \tag{7.25}$$

When Equation (7.25) is constrained, the following spurious constraint conditions appear: $a_5\to0$; $b_5\to0$; $a_8\to0$ and $b_8\to0$.

Our arguments projecting these as the cause of parasitic shear would be proved beyond doubt if we can derive a suitable error model. These error models are now much more difficult to construct, but have been achieved using a judicious mix of *a priori* and *a posteriori* knowledge of zero strain and stress conditions to simplify the problem. These error models have been convincingly verified by numerical computations [7.1].
A field-consistent representation will be one that ensures that the interpolations for the shear fields will contain only the consistent terms. A simple way to achieve this is to retain only the consistent terms from the original interpolations. Thus, for γ_{xy} we have,

$$\gamma_{xy} = (a_3 + b_2) + (a_6 + b_7)z \tag{7.26}$$

Similarly, the other shear strain fields can be modified. These strain fields should now be able to respond to bending modes in all three planes without locking.

7.4 Incompressible locking

Conventional displacement formulations of 2D plane strain and 3D elasticity fail when Poisson's ratio $\nu \to 0.5$, i.e. as the material becomes incompressible. Such situations can arise in modeling of material such as solid rocket propellants, saturated cohesive soils, plastics, elastomers and rubber like materials and in materials that flow, e.g. incompressible fluids or in plasticity. Displacement fields lock and highly oscillatory stresses are seen - drawing an analogy with shear and membrane locking, we can describe the phenomenon as *incompressible locking*. In fact, a penalty term (bulk modulus $\to \infty$ as $\nu \to 0.5$) is easily identifiable as enforcing incompressibility. Since this multiplies the volumetric strain, it is easy to argue that a lack of consistency in the definition of the volumetric strain will cause locking and will appear as oscillatory mean stresses or pressures.

7.4.1 A simple one-dimensional case - an incompressible hollow sphere

It is instructive to demonstrate how field-consistency operates in the finite element approximation of a problem in incompressible (or *nearly*-incompressible) elasticity by taking the simplest one-dimensional case possible. A simple problem of a pressurized elastic hollow sphere serves to illustrate this.

Consider an elastic hollow sphere of outer radius b and inner radius a with an internal pressure P. If the shear modulus G is 1.0, the radial displacement field for this case is given by,

$$u = \rho \left[\frac{1}{4r^2} + \frac{(1-2\nu)}{2(1+\nu)} r \right] \tag{7.27}$$

where $\rho = Pba^3 / \left[G\left(b^3 - a^3\right) \right]$ and $r = R/b$ non-dimensional radius and ν is the Poisson's ratio.

A finite element approximation approaches the problem from the minimum total potential principle. Thus, a radial displacement u leads to the following strains:

$$\varepsilon_r = u,_r \qquad \varepsilon_\theta = u/r \qquad \varepsilon_\phi = u/r$$

and the volumetric strain is

$$\varepsilon = \varepsilon_r + \varepsilon_\theta + \varepsilon_\phi = u,_r + 2u/r$$

The elastic energy stored in the sphere (when $G=1$) is

$$U = \int_{\bar{a}}^{1} \left(\varepsilon_r^2 + \varepsilon_\theta^2 + \varepsilon_\phi^2 + 1/2\,\alpha\, \varepsilon^2 \right) r^2 \, dr \tag{7.28}$$

and $\alpha = 2\nu/(1-2\nu)$ when $G=1$ and $\bar{a} = a/b$ is the dimensionless inner radius. The displacement type finite element representation of this very simple problem runs into a lot of difficulties when $\nu \to 0.5$, i.e., when $\alpha \to \infty$ in the functional represented by Equation (7.28).

These arguments now point to the volumetric strain field in Equation (7.28) as the troublesome term. When $\alpha \to \infty$, this strain must vanish. In a physical situation, and in an infinitesimal interpretation of Equation (7.28), this means that $\varepsilon \to 0$. However, when a finite element discretization is introduced, this does not happen so simply. To see this, let us examine what will happen when a linear element is used to model the problem.

7.4.2 Formulation of a linear element

The displacement field u and the radial distance r are interpolated by linear isoparametric functions as

$$r = 0.5(r_1 + r_2) + 0.5(r_2 - r_1)\xi \quad (7.29a)$$

$$u = 0.5(u_1 + u_2) + 0.5(u_2 - u_1)\xi \quad (7.29b)$$

where the nodes of the element are at r_1 and r_2.

The troublesome term in the potential energy functional is the volumetric strain and this contribution can be written as,

$$\int \varepsilon^2 r^2 \, dr = \int (r u_{,r} + 2u)^2 \, dr \quad (7.30)$$

It is the discretized representation of this term $(r u_{,r} + 2u)$ that will determine whether there will be locking when $\alpha \to \infty$. Thus, unlike in previous sections, the constraint is not on the volumetric strain ε but on $r\varepsilon$ because of the use of spherical coordinates to integrate the total strain energy. It is therefore meaningful to define this as a pseudo-strain quantity $\gamma = r\varepsilon$. To see how this is inconsistently represented, let us now write the interpolation for this derived kinematically from the displacement fields as,

$$(r u_{,r} + 2u) = \left[\frac{(r_1 + r_2)}{2(r_2 - r_1)} (u_2 - u_1) + (u_1 + u_2) \right] + \left[3/2 (u_2 - u_1) \right] \xi \quad (7.31)$$

Consider now the constraints that are enforced when this discretized field is used to develop the strain energy arising from the volumetric strain as shown in Equation (7.31) when $\alpha \to \infty$.

$$\frac{(r_1 + r_2)}{2(r_2 - r_1)} (u_2 - u_1) + (u_1 + u_2) \to 0 \quad (7.32a)$$

$$(u_2 - u_1) \to 0 \quad (7.32b)$$

Condition (7.32a) represents a meaningful discretized version of the condition of vanishing volumetric strain and is called a true constraint in our field-consistency terminology. However, condition (7.32b) leads to an undesired restriction on the u field as it implies $u_{,r} \to 0$. This is therefore the spurious constraint that leads to locking and spurious pressure oscillations.

7.4.3 Incompressible 3D elasticity

We now go directly to modeling with 3D elasticity. We re-write the strain energy for 3D elasticity in the following form:

$$U = 1/2\, G \int \varepsilon_d^T\, D\, \varepsilon_d\, dV + 1/2\, \lambda \int \varepsilon_n^T\, \varepsilon_n\, dV \tag{7.33}$$

In Equation (7.33), ε_d is the distortional strain and ε_n is the volumetric strain. In this form, it is convenient to describe the elasticity matrix in terms of the shear modulus, G and the bulk modulus K, where $G = E/[2(1+\nu)]$, $K = E/[3(1-2\nu)]$ and $\lambda = (K - 2G/3) = E\,\nu/[(1+\nu)(1-2\nu)]$.

Consider the fields given in Equations (7.24) for the 8-noded brick element. An elastic response for incompressible or nearly-incompressible materials will require a constrained strain field,

$$\varepsilon_n = u,_x + v,_y + w,_z \rightarrow 0 \tag{7.34}$$

where ε_n is the volumetric strain. From Equations (7.24) and (7.34) we have,

$$\varepsilon_n = (a_2 + b_3 + c_4) + (b_5 + c_7)x + (a_5 + c_6)y + (a_7 + b_6)z + (a_8 yz + b_z xz + c_8 xy) \tag{7.35}$$

Equation (7.35) can be constrained to zero only when the coefficients of each of its terms vanish, giving rise to the constraint conditions,

$$a_2 + b_3 + c_4 \rightarrow 0 \tag{7.36a}$$
$$b_5 + c_7 \rightarrow 0 \tag{7.36b}$$
$$a_5 + c_6 \rightarrow 0 \tag{7.36c}$$
$$a_7 + b_6 \rightarrow 0 \tag{7.36d}$$
$$a_8 \rightarrow 0 \tag{7.36e}$$
$$b_8 \rightarrow 0 \tag{7.36f}$$
$$c_8 \rightarrow 0 \tag{7.36g}$$

Equation (7.36b) to (7.36) are the inconsistent terms that cause locking. To ensure a field-consistent representation, only the consistent terms should be retained, giving

$$\varepsilon_n = a_2 + b_3 + c_4 \tag{7.37}$$

This field will now be able to respond to the incompressible or nearly incompressible strain states and the element should be free of locking.

7.4.4 Concluding remarks

It is clear from this section that incompressible locking is analogous to shear locking, etc. A robust formulation must therefore ensure consistent representations of volumetric strain in cases where incompressibility or near incompressibility is expected.

7.5 References

7.1 G. Prathap, *The Finite Element Method in Structural Mechanics*, Kluwer Academic Press, Dordrecht, 1993.